

LOW EARTH ORBIT SOUNDER RETRIEVAL
PRODUCTS AT GEOSTATIONARY EARTH ORBIT
SPATIAL AND TEMPORAL SCALES

By

James F. Anheuser

A thesis submitted in partial fulfillment of the
requirements for the degree of

Master of Science
(Atmospheric and Oceanic Science)

At the

UNIVERSITY OF WISCONSIN-MADISON
2020

Abstract

Low Earth Orbit Sounder Retrieval Products at Geostationary Earth Orbit Spatial and Temporal Scales

By

James F. Anheuser

Infrared hyperspectral sounders, onboard satellites in low Earth orbit, are high spectral resolution interferometers capable of providing very accurate infrared radiance measurements using thousands of channels. Though their temporal resolution is a relatively low 12 hours, these data can be used to produce high vertical resolution temperature and humidity profiles. Imagers are radiometers providing high spatial resolution and, when aboard satellites in geostationary Earth orbit, high temporal resolution radiance measurements across a more limited number of bands, typically ~ 10 to ~ 20 . Their data are used for monitoring Earth's weather and climate. Here, a data fusion method (developed and previously demonstrated at UW-Madison) is utilized to construct high vertical resolution, sounder-like temperature and humidity retrievals at imager high spatial and temporal resolution. Using the Crosstrack Infrared Sounder and Advanced Baseline Imager, parameters of the process are explored, a case study is demonstrated and initial validation is presented. Fusion to radiosonde comparison from Feb. 2017– Feb. 2018 over Department of Energy Atmospheric Radiation Measurement Southern Great Plains Site shows a temperature bias in the troposphere is $\sim -2\text{K}$ with a standard deviation of ~ 2 and relative humidity bias in the tropopause is ~ 0 with a standard deviation of $\sim 0.1\%$.

Table of Contents

<i>Abstract</i>	<i>i</i>
Low Earth Orbit Sounder Retrieval Products at Geostationary Earth Orbit Spatial and Temporal Scales	<i>i</i>
<i>Table of Figures</i>	<i>iii</i>
<i>I. Introduction</i>	<i>1</i>
<i>II. Fusion Process Methods and Results</i>	<i>8</i>
a. K-d Tree Search	<i>9</i>
b. Retrieval Fusion	<i>10</i>
c. Optimization	<i>12</i>
d. Product Fusion.....	<i>19</i>
e. Product Fusion Time Series	<i>24</i>
<i>III. Validation</i>	<i>27</i>
a. Radiosonde Dataset	<i>28</i>
b. Product Fusion Dataset	<i>30</i>
c. Results.....	<i>31</i>
<i>IV. Summary and Conclusion</i>	<i>33</i>
<i>Bibliography</i>	<i>36</i>

Table of Figures

Figure 1: Cross Track Infrared Sounder (CrIS) derived temperature retrievals at 300 hPa (left) and 500 hPa (right) over the Chesapeake Bay region at 1754Z on May 19 th , 2017 created using the University of Wisconsin Dual Regression (UW DR) retrieval algorithm [7]. The data contains vertical information about the temperature field albeit at low horizontal resolution. Cloud detection and cloud products are also retrieved— cloudy FOVs are not plotted.	3
Figure 2: Cross Track Infrared Sounder derived temperature and humidity retrieval profile at 36.6N, -97.6W at 1902Z on July 29 th , 2018 created using the University of Wisconsin Dual Regression (UW DR) retrieval algorithm [7]. Resolution of vertical properties of atmospheric characteristics is the intent of high spectral resolution sensors such as CrIS.	3
Figure 3: Advanced Baseline Imager (ABI) brightness temperatures from channel 8 (left) and channel 15 (right) taken aboard Geostationary Operational Environmental Satellite (GOES)-16 over the Chesapeake Bay region at 1800Z on May 19 th , 2017. Channel 8 is known as the “upper level water vapor” band and channel 15 is known as the “dirty longwave window band” [15]. These images exhibit the high horizontal resolution of imagers.....	5
Figure 4: Mid-level water vapor across North America represented by the Advanced Baseline Imager (ABI) brightness temperatures from channel 9 taken aboard Geostationary Operational Environmental Satellite (GOES)-16 at 17:10 GMT on November 12 th , 2019. Data available via University of Wisconsin Atmospheric, Oceanic and Space Sciences (https://www.aos.wisc.edu/weather/wx_obs/Satellite.html). Imager channels typically correspond to a general atmospheric characteristic such as “mid-level water vapor” rather than to exact layers within the atmosphere.	6
Figure 5: Example Crosstrack Infrared Sounder (CrIS) observed brightness temperature spectrum (blue, left axis) and Advanced Baseline Imager (ABI) infrared channel spectral response functions (red, right axis) plotted versus wavenumber. The sounder is able to resolve the brightness temperature spectrum in much greater detail than the imager.....	7
Figure 6: The imager pixel to sounder FOV match process shown in flowchart form. Adapted from Fusion of satellite-based imager and sounder data to construct supplementary high spatial resolution narrowband IR radiances by Elisabeth et. al, 2017, Journal of Applied Remote Sensing, 11(3), p. 14. The imager radiances at native geolocation and spatial resolution (HIRES) and at sounder geolocation and spatial resolution (LORES) are inputs to a k-d search tree method used to match each imager pixel to a subset of N closest match sounder fields of view (FOVs).....	9
Figure 7: Example Advanced Baseline Imager (ABI) channel 8 radiances at native geolocation and spatial resolution (left) and at Crosstrack Infrared Sounder (CrIS) overpass geolocation and spatial resolution (right). These two datasets serve, respectively, as the query and training data set	

inputs to the k-d tree used to match each imager pixel to a subset of N closest match sounder fields of view (FOVs).....	11
Figure 8: The locations of an example imager pixel (blue x) and it's best match sounder fields of view (blue circle) found via a k-d tree search tree (left) along with the temperature and dew point retrieval profiles corresponding to the best match sounder fields of view (center) and the resultant fusion temperature and dew point profiles for the imager pixel in question (left). The best match sounder FOV retrievals are averaged to construct the fusion retrieval.....	12
Figure 9: Fusion temperature at 850 hPa (top), 500 hPa (second from top) and 300 hPa (third from top) and fusion water vapor mixing ratio at 850 hPa (second from bottom) and 500 hPa (bottom) for N values of 5 (left), 10 (center) and 20 (right) over Chesapeake Bay using the Advanced Baseline Imager (ABI) image from 1800Z and the Crosstrack Infrared Sounder (CrIS) data from the 1748Z and 1754Z granules. White signifies the presence of cloud at that pressure level. The data is horizontally smoothed as the N number increases.	14
Figure 10: Fusion temperature at 850 hPa (top), 500 hPa (second from top) and 300 hPa (third from top) and fusion water vapor mixing ratio at 850 hPa (second from bottom) and 500 hPa (bottom) for minimum clear matched fields of view (FOVs) of one (left) and two (right) over Chesapeake Bay using the Advanced Baseline Imager (ABI) image from 1800Z and the Crosstrack Infrared Sounder (CrIS) data from the 1748Z and 1754Z granules. White signifies the presence of cloud at that pressure level. Outlier values are reduced when the restriction is increased from one to two.	16
Figure 11: Fusion temperature at 850 hPa (top), 500 hPa (second from top) and 300 hPa (third from top) and fusion water vapor mixing ratio at 850 hPa (second from bottom) and 500 hPa (bottom) using two Advanced Baseline Imager (ABI) channels (14 and 15, left), six ABI channels (two channels plus 8, 9, 10 and 16, center) and eight ABI channels (six channels plus 11 and 12, right) over Chesapeake Bay using the Advanced Baseline Imager (ABI) image from 1800Z and the Crosstrack Infrared Sounder (CrIS) data from the 1748Z and 1754Z granules. White signifies the presence of cloud at that pressure level. Additional channels in the fusion process improve the result.	18
Figure 12: Advanced Baseline Imager (ABI) brightness temperatures from channels 8 (top left), 9 (top center), 10 (top right), 11 (middle left), 12 (middle center), 14 (middle right), 15 (bottom left) and 16 (bottom right) taken aboard Geostationary Operational Environmental Satellite (GOES)- 16 over the Chesapeake Bay region at 1800Z on May 19 th , 2017. These images serve as the imager input into the fusion process example shown here.	20
Figure 13: Cross Track Infrared Sounder (CrIS) derived temperature retrievals at 300 hPa (top, left), 500 hPa (top, center) and 850 hPa (top, right) and water vapor mixing ratio retrievals at 500 hPa (bottom, left) and 850 hPa (bottom, right) over the Chesapeake Bay region at 1754Z on May 19 th , 2017 created using the University of Wisconsin Dual Regression (UW DR) retrieval algorithm [7]. These data serve as the sounder input into the fusion process example shown here.	21
Figure 14: Fusion temperature retrievals at 300 hPa (top, left), 500 hPa (top, center) and 850 hPa (top, right) and water vapor mixing ratio retrievals at 500 hPa (bottom, left) and 850 hPa (bottom, right) over the Chesapeake Bay region at 1754Z on May 19 th , 2017 created using the Advanced Baseline Imager (ABI) and University of Wisconsin Dual Regression (UW DR) retrieval algorithm [7] applied to Crosstrack Infrared Sounder (CrIS) radiances.....	22
Figure 15: Locations of a special sonde launch, nearest fusion pixel, best match sounder fields of view (FOVs) and nearest CrIS FOV overlayed on 850 hPa dew point temperature at 1800Z on	

May 19 th , 2017 over eastern North America (left). Vertical profiles of temperature and dew point temperatures of the special sonde, nearest fusion pixel, nearest CrIS FOV retrieval and National Centers for Environmental Prediction (NCEP) Rapid Refresh (RAP) model [22] nearest gridbox (right). The fusion profile matches the sonde more closely than the CrIS retrieval.....	23
Figure 16: Fusion temperature at 850 hPa (top), 500 hPa (second from top) and 300 hPa (third from top) and fusion water vapor mixing ratio at 850 hPa (second from bottom) and 500 hPa (bottom) at 1800Z (left), at 2000Z (center) and at 2200Z (right) over Chesapeake Bay using the Advanced Baseline Imager (ABI) image from 1800Z and the Crosstrack Infrared Sounder (CrIS) data from the 1748Z and 1754Z granules. White signifies the presence of cloud at that pressure level. Features in the atmosphere, especially convective lift shown by the 500 hPa temperature (bold box), can be followed over time.	26
Figure 17: Temperature (left) and relative humidity (right) differences between sonde pairs launched ~60 minutes apart during day (top) and night (bottom) at the Department of Energy (DOE) Atmospheric Radiation Measurement (ARM) Southern Great Plains (SGP) site [21] during the validation campaign for the Atmospheric Infrared Sounder (AIRS). Adapted from Atmospheric Radiation Measurement site atmospheric state best estimates for Atmospheric Sounder temperature and water vapor retrieval validation by Tobin et al., 2006, Journal of Geophysical Research-Atmospheres, 111(D9), p. 18. These figures quantify the atmospheric variability a radiosonde can experience during the duration of its ascent through the atmosphere.	29
Figure 18: Left— Mean (solid) and standard deviation (dashed) of temperature differences versus pressure level for sonde and fusion (black), model and fusion (blue) and sounder and sonde (orange) from Feb. 2017- Feb. 2018 over DOE ARM SGP Site. Right— number of clear samples versus pressure level for the period in question. Temperature bias in the troposphere is ~-2K with a standard deviation of ~2K.	32
Figure 19: Left— Mean (solid) and standard deviation (dashed) of relative humidity differences versus pressure level for sonde and fusion (blue) and model and fusion (orange) from Feb. 2017- Feb. 2018 over DOE ARM SGP Site. Right— number of clear samples versus pressure level for the period in question. Relative humidity bias in the tropopause is ~0 with a standard deviation of ~0.1%.....	33

I. Introduction

Data fusion is “the integration of data and knowledge from several sources” [1]. In other words, it is the process by which synergy is identified and utilized between two unique data sources. In the context of this work, data fusion entails “fusing” two satellite data sets together in such a way that the resulting product exhibits the unique advantages and sheds the unique disadvantages of each data set individually. I.e., the whole of the fusion dataset is greater than the metaphoric sum of the parts. Data fusion in remote sensing is not a new concept and has been used in various forms to construct infrared imager channels from infrared sounder observations to maintain continuity [2], to construct true color imagery when the green radiances are not available [3] and to produce high spatial and temporal resolution surface reflectance products [4]. In the coming era of smaller satellites and more specialized platforms [5], the importance of utilizing synergies across instruments and platforms will only grow.

High-spectral resolution (or hyperspectral) infrared sounders (sounders) allow better determination of vertical profiles of atmospheric characteristics owing to their unmatched, very high spectral resolution and number of channels (Table 2). A typical hyperspectral infrared sounder has thousands of channels meaning it is sensitive to brightness temperature differences across very narrow spectral bands that are very accurately calibrated [6]. Figure 5 illustrates the spectral brightness temperature detail that can be resolved from a hyperspectral sounder observation. It is within these details that vertical information can be derived using a retrieval algorithm such as the University of Wisconsin Dual Regression (UW DR) retrieval algorithm available through the University of Wisconsin Cooperative Institute for Meteorological Satellite

Studies Community Satellite Processing Package [7, 8]. While there are many other types of hyperspectral sounder retrieval methods (optimal estimation, e.g.), the UW DR algorithm is based on linear regression [7, 8]; non-linearities are addressed using classified statistics and decision steps. The algorithm provides atmospheric profiles and surface and cloud parameters under clear and cloudy sky conditions at single field of view (FOV) horizontal resolution. In general, hyperspectral sounder algorithms are capable of retrieving vertical temperature and humidity profiles with an accuracy of 1 deg K and 20% humidity, respectively, within a 1 km layer [9, 10]. The information from these vertical profiles, such as the examples shown in Figures 1 and 2, can be used for forecasting, model assimilation and research [11].

Many sounders, such as the Crosstrack Infrared Sounder (CrIS) aboard Suomi NPP and the Joint Polar Satellite System (JPSS) series [12], are aboard polar orbiting satellites [13, 14]. This means while their radiance data are available from the entire globe, most notably in regions where observations are sparse, its ~12 hour temporal resolution is low (Table 2). Additionally, sounders have large a FOV size, typically ~14 km. This limits the ability of sounders to provide the type of time evolution or high horizontal resolution information often used in nowcasting type settings.

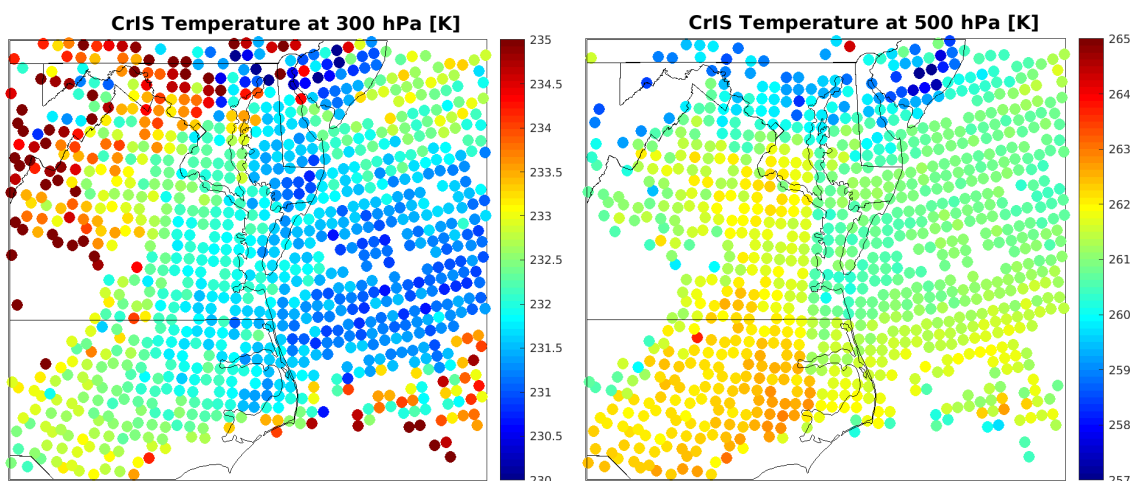


Figure 1: Cross Track Infrared Sounder (CrIS) derived temperature retrievals at 300 hPa (left) and 500 hPa (right) over the Chesapeake Bay region at 1754Z on May 19th, 2017 created using the University of Wisconsin Dual Regression (UW DR) retrieval algorithm [7]. The data contains vertical information about the temperature field albeit at low horizontal resolution. Cloud detection and cloud products are also retrieved—cloudy FOVs are not plotted.

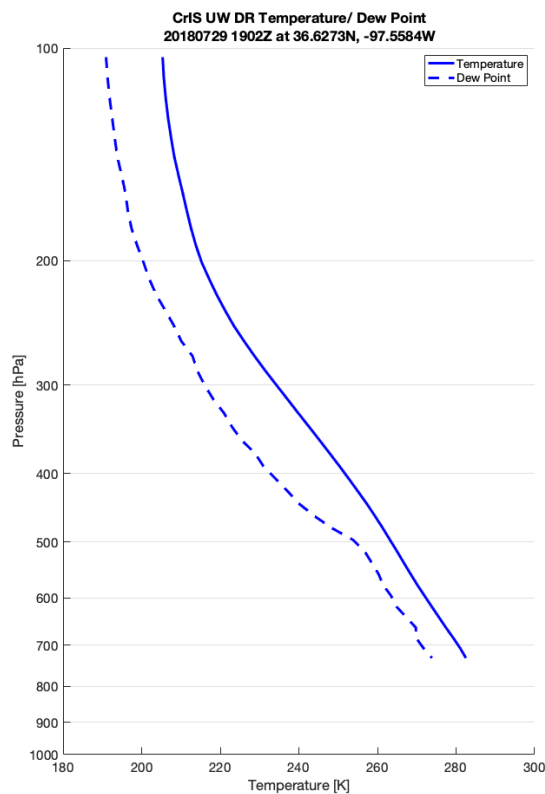


Figure 2: Cross Track Infrared Sounder derived temperature and humidity retrieval profile at 36.6N, -97.6W at 1902Z on July 29th, 2018 created using the University of Wisconsin Dual Regression (UW DR) retrieval algorithm [7]. Resolution of vertical properties of atmospheric characteristics is the intent of high spectral resolution sensors such as CrIS.

Infrared imagers (imagers) use a much lower number of channels compared to sounders to provide information about particular characteristics of the atmosphere (Table 1, Figure 4). A typical imager has roughly 10 infrared channels, with each channel often corresponding to a particular characteristic such as mid-level water vapor or ozone [15]. The lack of spectral resolution, however, limits a typical imagers ability to create high vertical resolution profiles of atmospheric characteristics. In Figure 5, the spectral response functions of 10 infrared channels are plotted and show the enormous relative lack of spectral resolution exhibited by an imager versus a sounder.

Table 1: Advanced Baseline Imager (ABI) visible, near infrared and infrared bands and their nicknames. Adapted from Applications of the 16 Spectral Bands on the Advanced Baseline Imager (ABI), Tim Schmit, et al., 2018, Journal of Operational Meteorology, 6(4), p. 33–46. The nicknames correspond to the atmospheric characteristic that each channel is designed to observe.

Central Wavelength	Band Number	Type	Nickname
0.47	1	Visible	Blue
0.64	2	Visible	Red
0.86	3	Near- Infrared	Veggie
1.37	4	Near- Infrared	Cirrus
1.6	5	Near- Infrared	Snow/ Ice
2.2	6	Near- Infrared	Cloud Particle Size
3.9	7	Infrared	Shortwave Window
6.2	8	Infrared	Upper- level Water Vapor
6.9	9	Infrared	Mid-level Water Vapor
7.3	10	Infrared	Low- level Water Vapor
8.4	11	Infrared	Cloud- Top Phase
9.6	12	Infrared	Ozone
10.3	13	Infrared	“Clean” Longwave Window
11.2	14	Infrared	Longwave Window
12.3	15	Infrared	“Dirty” Longwave Window
13.3	16	Infrared	CO ₂

In contrast to spectral or vertical resolution, imagers often can have very high horizontal resolution (Table 2)—sometimes on the order of hundreds of meters. Imagers have much higher horizontal resolution than sounders, typically $\sim 2\text{km}$ or less at nadir [16, 17] as seen in Figure 3. This allows for the resolution of spatially small features in the atmosphere such as overshooting tops in a developing convective system [18]. Imagers, such as the Advanced Baseline Imager (ABI), are often aboard geostationary satellites. While these platforms are limited to a single viewing angle and cannot view the high latitudes, they are able to provide much higher temporal resolution, sometimes as high as one minute [15]. This makes imagers ideal for providing the type of high temporal and spatial resolution information used in nowcasting settings, albeit without highly resolved vertical information or information from the polar regions.

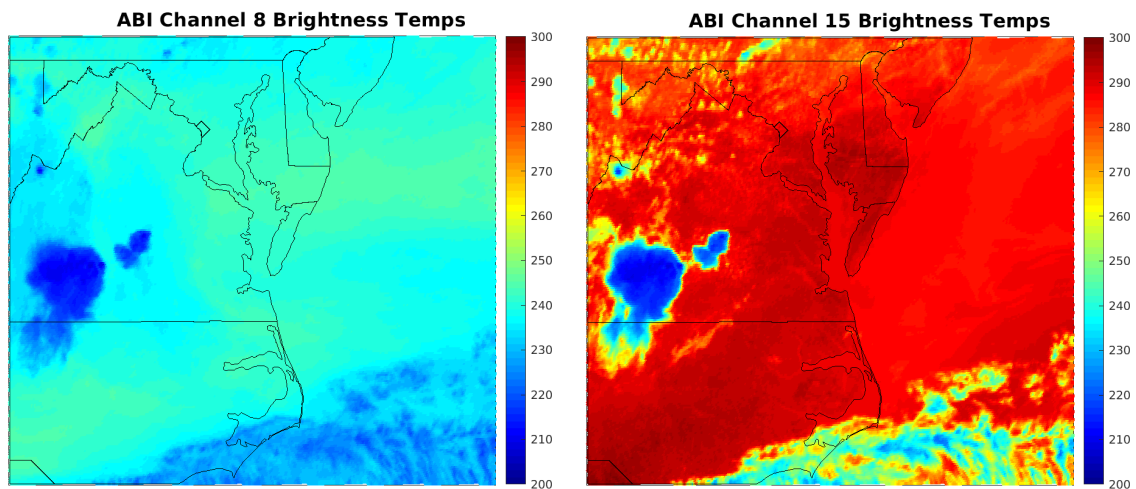


Figure 3: Advanced Baseline Imager (ABI) brightness temperatures from channel 8 (left) and channel 15 (right) taken aboard Geostationary Operational Environmental Satellite (GOES)-16 over the Chesapeake Bay region at 1800Z on May 19th, 2017. Channel 8 is known as the “upper level water vapor” band and channel 15 is known as the “dirty longwave window band” [15]. These images exhibit the high horizontal resolution of imagers.

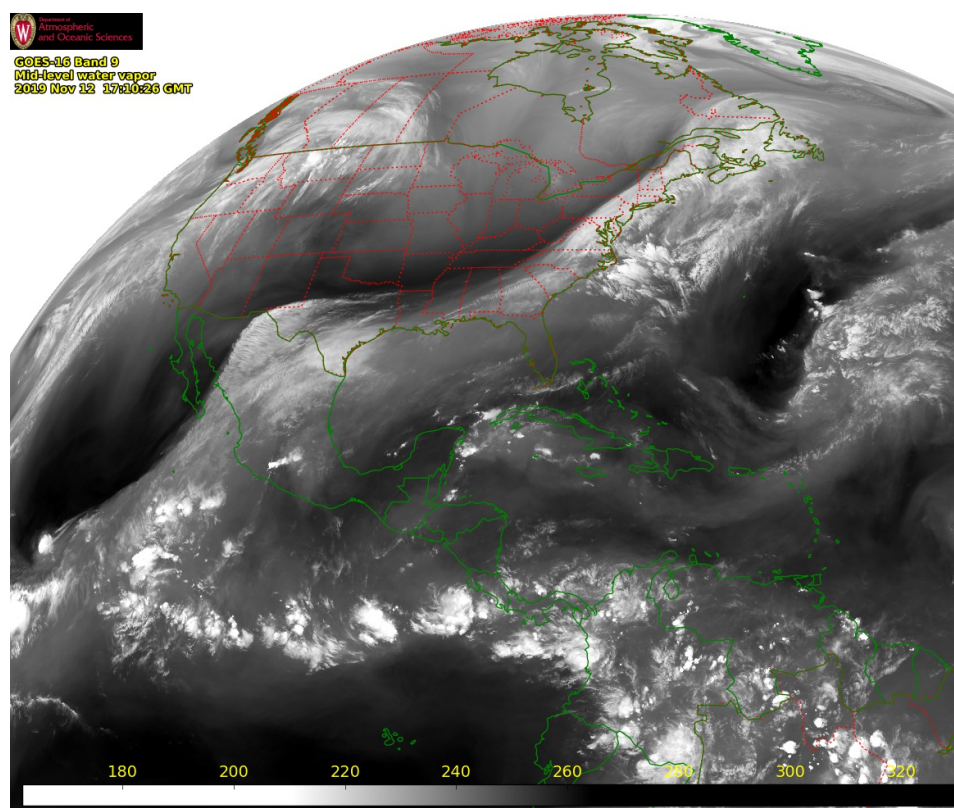


Figure 4: Mid-level water vapor across North America represented by the Advanced Baseline Imager (ABI) brightness temperatures from channel 9 taken aboard Geostationary Operational Environmental Satellite (GOES)-16 at 17:10 GMT on November 12th, 2019. Data available via University of Wisconsin Atmospheric, Oceanic and Space Sciences (https://www.aos.wisc.edu/weather/wxs_obs/Satellite.html). Imager channels typically correspond to a general atmospheric characteristic such as “mid-level water vapor” rather than to exact layers within the atmosphere.

The synergy utilized here will be the complementing vertical, horizontal and temporal resolutions of infrared imagers and sounders (Table 2). The final product will be a retrieval product that has the vertical resolution of an infrared sounder ($\sim 1\text{km}$) and the horizontal and temporal resolutions of an infrared imager (3 to 4 km over CONUS and one minute, respectively). Infrared sounder/imager fusion has been proven to construct radiances with sounder type spectral resolution at geostationary imager temporal and horizontal resolution [19]. When applied directly to the hyperspectral sounder retrievals rather than radiances, sounder/imager fusion allows construction of the aforementioned high vertical resolution, sounder like retrievals at geostationary imager temporal and horizontal resolution [20]. As such,

sounder/imager fusion offers improvements over both sounder and imager data alone and has potential for use in nowcasting or research settings, among others. The sounder/imager fusion process involves a number of flexible parameters that are explored herein using CrIS/ABI retrieval fusion.

Table 2: Summary of Cross Track Infrared Sounder (CrIS) and Advanced Baseline Imager (ABI) attributes. Adapted from Imager and sounder data fusion to generate sounder products at an improved spatial and temporal resolution Elisabeth Weisz and Paul Menzel, 2019, Journal of Applied Remote Sensing, 13(3), p. 12. CrIS has a much higher number of channels than ABI while ABI has a much smaller field of view (FOV) size at nadir.

Instrument	Satellite	IR spectral range (μm)	No. of IR channels	FOV size (nadir)	Swath width	Scanning
CrIS	S-NPP, NOAA-20	3.9–15.4	1305 (NSR) 2211 (FSR)	14 km	2200 km	± 48.5 deg
ABI	GOES-16, -17	3.9–13.3	10	2 km	Full disk	

Note: NSR, normal spectral resolution; FSR: full spectral resolution.

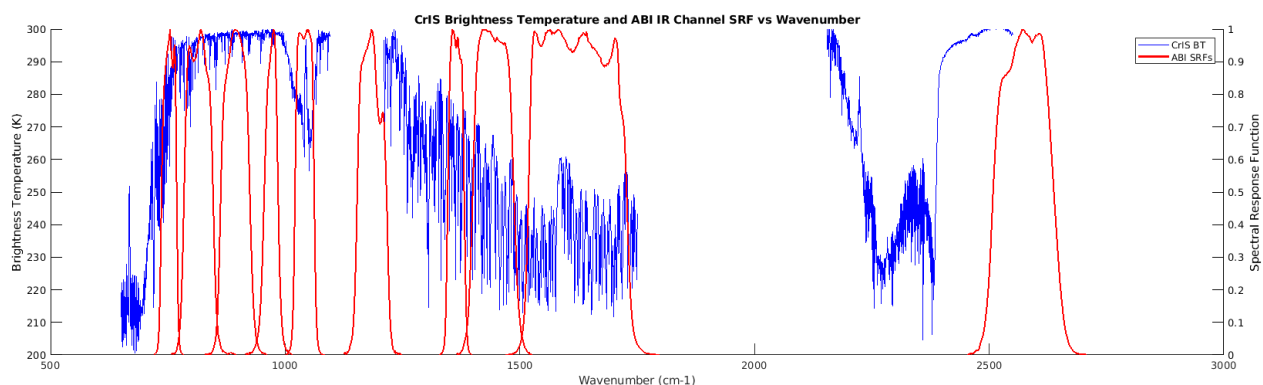


Figure 5: Example Cross-track Infrared Sounder (CrIS) observed brightness temperature spectrum (blue, left axis) and Advanced Baseline Imager (ABI) infrared channel spectral response functions (red, right axis) plotted versus wavenumber. The sounder is able to resolve the brightness temperature spectrum in much greater detail than the imager.

Sounder/imager fusion as applied to radiances has been validated against legacy channels available on MODIS [19], leading to the expectation that sounder/imager fusion as applied to retrievals will contain reasonably accurate and useful information. In this work, we provide statistical validation of sounder/imager retrieval fusion results using radiosonde data provided by the Department of Energy (DOE) Atmospheric Radiation Measurement (ARM) facility [21] and model data from the National Oceanic and Atmospheric Association (NOAA) National Centers for Environmental Prediction (NCEP) Rapid Refresh (RAP) model [22]. We also discuss a number of case studies from these radiosonde launches as well as a scene from the mid-Atlantic that further illustrate sounder/imager fusion capabilities.

II. Fusion Process Methods and Results

The fusion process described herein has been utilized to construct both radiances [19] and retrievals [20]. A k-d tree search algorithm applied to imager radiance and geolocation is used to find some number (N) of closest matching (in radiance and geolocation space) sounder FOVs for each imager pixel. The sounder and imager data need not be concurrent, though near concurrent is favorable for a real time image. In radiance fusion, the radiances of these N closest match FOVs are averaged for each pixel to construct fusion radiances. In retrieval fusion as demonstrated here, the retrievals corresponding to the N closest match sounder FOVs are averaged at every pressure level to construct retrievals corresponding to each imager pixel. The resulting fusion retrievals show the characteristics of the atmosphere at the vertical resolution of the sounder and at the horizontal resolution and time of the imager data. Various combinations of k-d tree search method parameters were explored and the resulting retrievals are presented in

this section. All plots and illustrations shown in the section were created using CrIS granules starting at 1748 UTC and 1754 UTC on May 19th 2017 over the Chesapeake Bay, VA region and the GOES-16 ABI images taken from 1800Z to 2100Z on the same day.

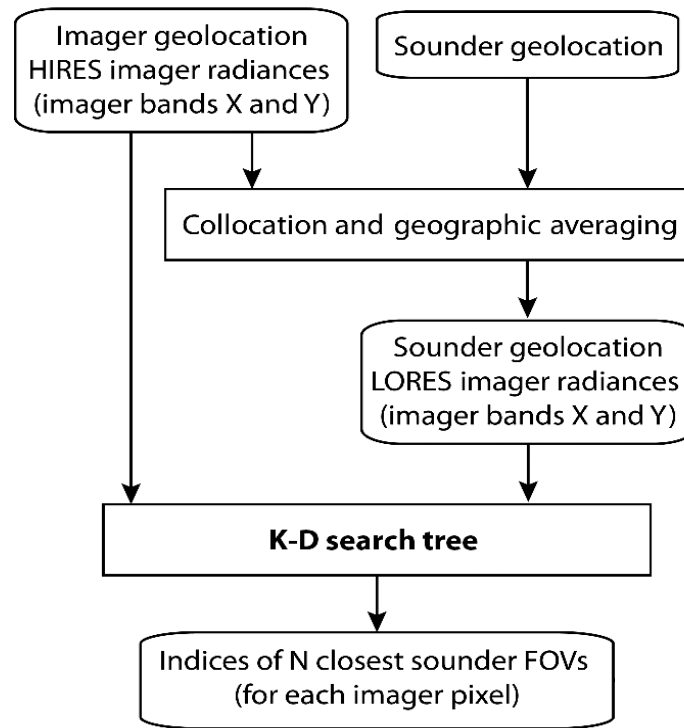


Figure 6: The imager pixel to sounder FOV match process shown in flowchart form. Adapted from Fusion of satellite-based imager and sounder data to construct supplementary high spatial resolution narrowband IR radiances by Elisabeth et. al, 2017, Journal of Applied Remote Sensing, 11(3), p. 14. The imager radiances at native geolocation and spatial resolution (HIREs) and at sounder geolocation and spatial resolution (LORES) are inputs to a k-d search tree method used to match each imager pixel to a subset of N closest match sounder fields of view (FOVs).

a. K-d Tree Search

A k-d tree search algorithm is used to find matches among the vectors of a training dataset to vectors within a query dataset [23]. It is a computationally fast and efficient method that can be applied to spaces of arbitrary dimensionality [23]. It is a search framework for which several programming languages have a built-in function or routine.

b. Retrieval Fusion

Here, imager pixel geolocation and radiance data form the query dataset (Figure 7, left). The imager pixels are geographically collocated to the sounder FOVs and the radiances are averaged within each FOV to form the training dataset (Figure 7, right). In other words, high and low resolution imager data form the query and training datasets, respectively. The k-d tree algorithm is then used to match each imager pixel from the query dataset with a set of N best match FOVs represented by the low resolution imager data in the training dataset. The sounder radiances themselves are not included in the search process. A cloudmask can be applied to the imager data prior to this process which saves computing time by eliminating pixels from the query dataset that are known to be cloudy. In this case, a cloudmask has been applied to the ABI data [24].

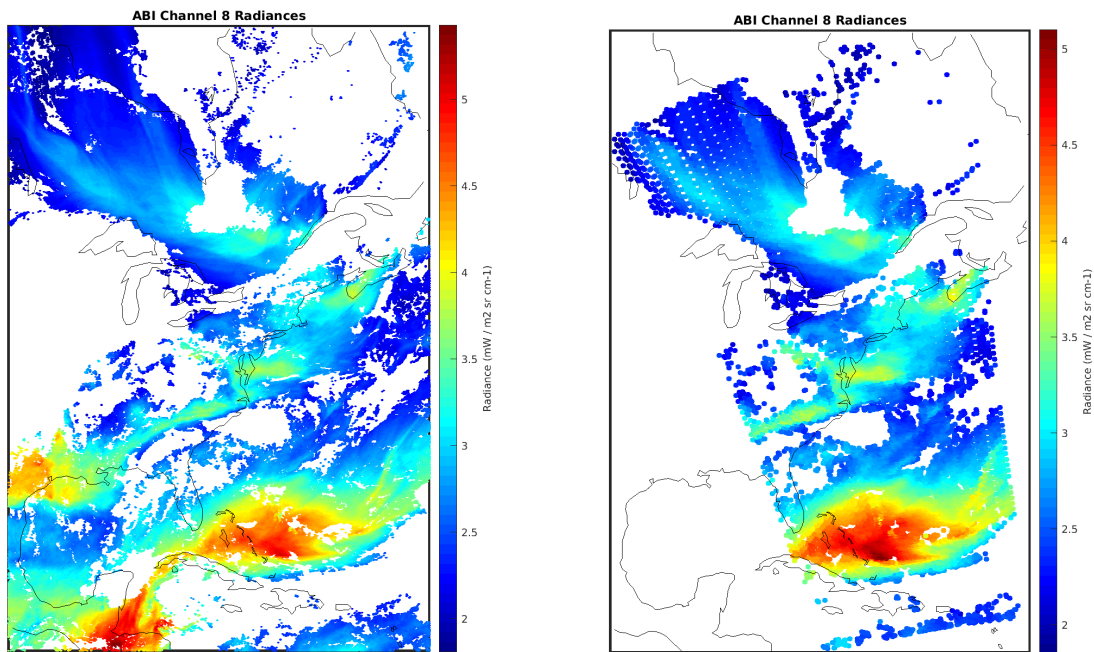


Figure 7: Example Advanced Baseline Imager (ABI) channel 8 radiances at native geolocation and spatial resolution (left) and at Crosstrack Infrared Sounder (CrIS) overpass geolocation and spatial resolution (right). These two datasets serve, respectively, as the query and training data set inputs to the k -d tree used to match each imager pixel to a subset of N closest match sounder fields of view (FOVs).

Next, the N retrievals corresponding to the N best match FOVs for each pixel are averaged at each pressure level (Figure 8). The result is a retrieval profile for every imager pixel. A minimum number of non-cloudy neighbors out of N for each pixel at a given pressure level is set, below which the pixel will be assigned as cloudy at the pressure level in question. Again, the sounder radiances themselves are not included in this step. However, this new data retains the high vertical resolution of the sounder derived retrieval along with the high horizontal resolution of the imager.

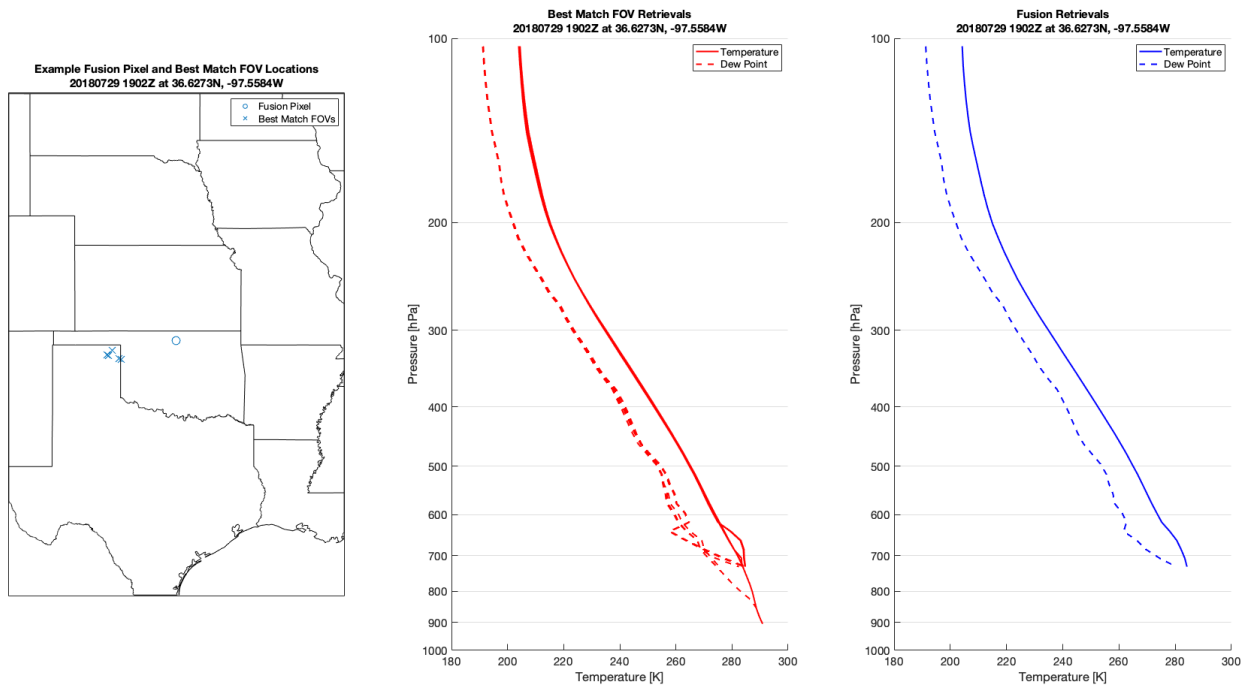


Figure 8: The locations of an example imager pixel (blue x) and its best match sounder fields of view (blue circle) found via a k -d tree search tree (left) along with the temperature and dew point retrieval profiles corresponding to the best match sounder fields of view (center) and the resultant fusion temperature and dew point profiles for the imager pixel in question (right). The best match sounder FOV retrievals are averaged to construct the fusion retrieval.

c. Optimization

Several aspects of the fusion process need to be quantitatively defined for actual implementation— the imager channel subset used, the number of N sounder FOVs output from the k -d tree search algorithm and the minimum number clear neighbors out of N for a pixel to be considered clear. Indeed, each of these parameters can be arbitrarily set and must be optimized— the results of which may differ depending on the constructed retrievals desired. Here, we optimize these parameters with temperature and water vapor retrievals in mind using

the combination of ABI imager aboard the geostationary platform GOES-16 and CrIS sounder aboard the polar orbiting platform Suomi NPP.

First, the value of N can be varied. A higher N tends to smooth spatial variation within the retrievals by including more data in the averaging while a lower N leads to greater spatial variation through the opposite mechanism. Higher values of N also reduce the chance of spurious results by including more samples in the averaging process. N values of 5, 10 and 20 were tried and results are shown in Figure 9. The fusion results created using $N=5$ exhibit a balance between spatial variation and sample size. The remaining fusion retrievals in this paper will use an N value of 5.

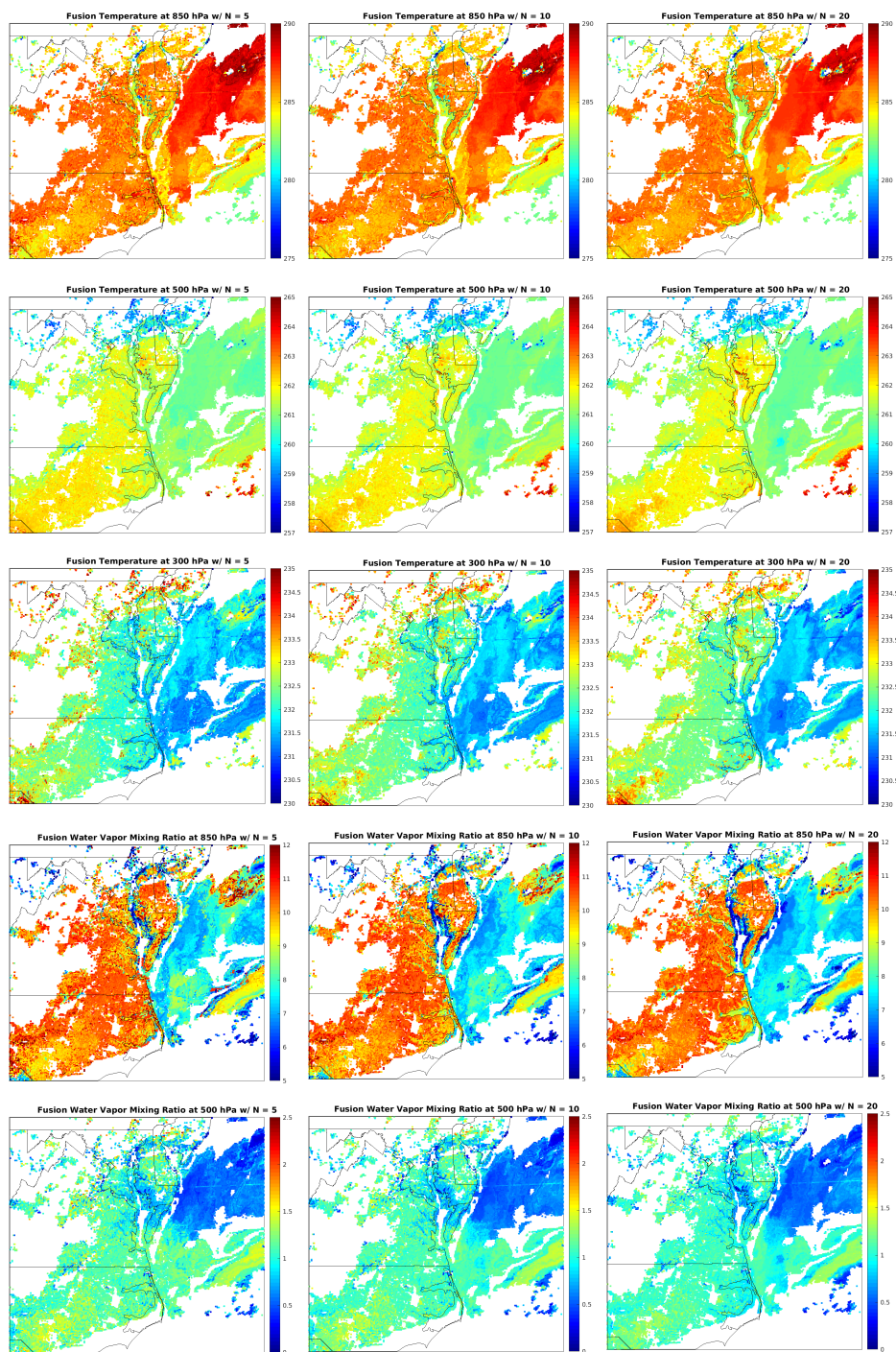


Figure 9: Fusion temperature at 850 hPa (top), 500 hPa (second from top) and 300 hPa (third from top) and fusion water vapor mixing ratio at 850 hPa (second from bottom) and 500 hPa (bottom) for N values of 5 (left), 10 (center) and 20 (right) over Chesapeake Bay using the Advanced Baseline Imager (ABI) image from 1800Z and the Cross-track Infrared Sounder (CrIS) data from the 1748Z and 1754Z granules. White signifies the presence of cloud at that pressure level. The data is horizontally smoothed as the N number increases.

Another parameter that can be varied is the minimum number of clear retrievals within the N best match FOV subset required to designate a pixel as clear. This requirement is applied at each pressure level. Allowing this parameter to be one allows a single retrieval from the N best match FOV subset to sway the resultant fusion retrieval; i.e., if four of the five best match FOVs are cloudy at a given pressure level, the remaining FOV becomes the fusion retrieval. There is a fair chance this fusion retrieval is erroneous and the pixel is in fact cloudy at that pressure level. Increasing this minimum reduces the clear pixels within the fusion retrieval at a given pressure level but also reduces spurious results. The best balance of these factors is achieved by setting this parameter to 2. A minimum number of clear retrievals within the N best match FOV subset required to designate a pixel as clear will be 2 for the remainder of this work.

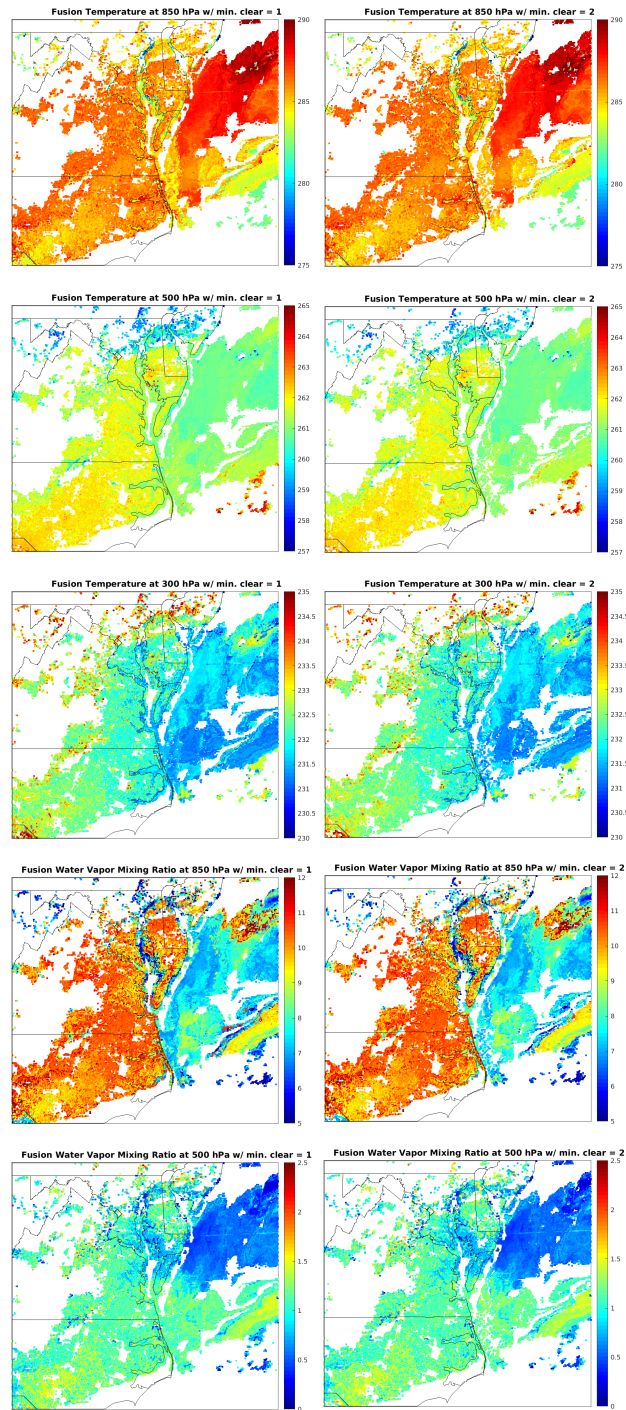


Figure 10: Fusion temperature at 850 hPa (top), 500 hPa (second from top) and 300 hPa (third from top) and fusion water vapor mixing ratio at 850 hPa (second from bottom) and 500 hPa (bottom) for minimum clear matched fields of view (FOVs) of one (left) and two (right) over Chesapeake Bay using the Advanced Baseline Imager (ABI) image from 1800Z and the Cross-track Infrared Sounder (CrIS) data from the 1748Z and 1754Z granules. White signifies the presence of cloud at that pressure level. Outlier values are reduced when the restriction is increased from one to two.

The ABI channels used as inputs may also be varied. Initially, the classical combination of longwave and dirty longwave channels was used. For ABI, this is channels 14 and 15 (Table 1). These results demonstrate the viability of this fusion approach and do contain good physical temperature and water vapor results (Figure 11, left). The k-d tree search process allows for any number of input dimensions as desired, so additional ABI channel input combinations were explored. With the intent of capturing more water vapor information, the upper, mid and low level water vapor channels were added along with the carbon dioxide channel (Table 1) to form a six channel trial (Figure 11, center). An eight channel trial was also completed by adding the cloud top phase (band 11) and ozone (band 12) channels (Table 1) to the six channels listed previous (Figure 11, right). This eight channel input strategy is used henceforth in this work.

Interestingly, adding ABI water vapor channels into the search process allows the fusion process to capture more water vapor structure in the final result. Figure 11 shows this clearly as the water vapor retrievals completed using the ABI water vapor channels include more structure, especially at 500 hPa in the pre-convective environment located over north-central Virginia. This isn't unexpected however it is a confirmation that the fusion process is working as expected.

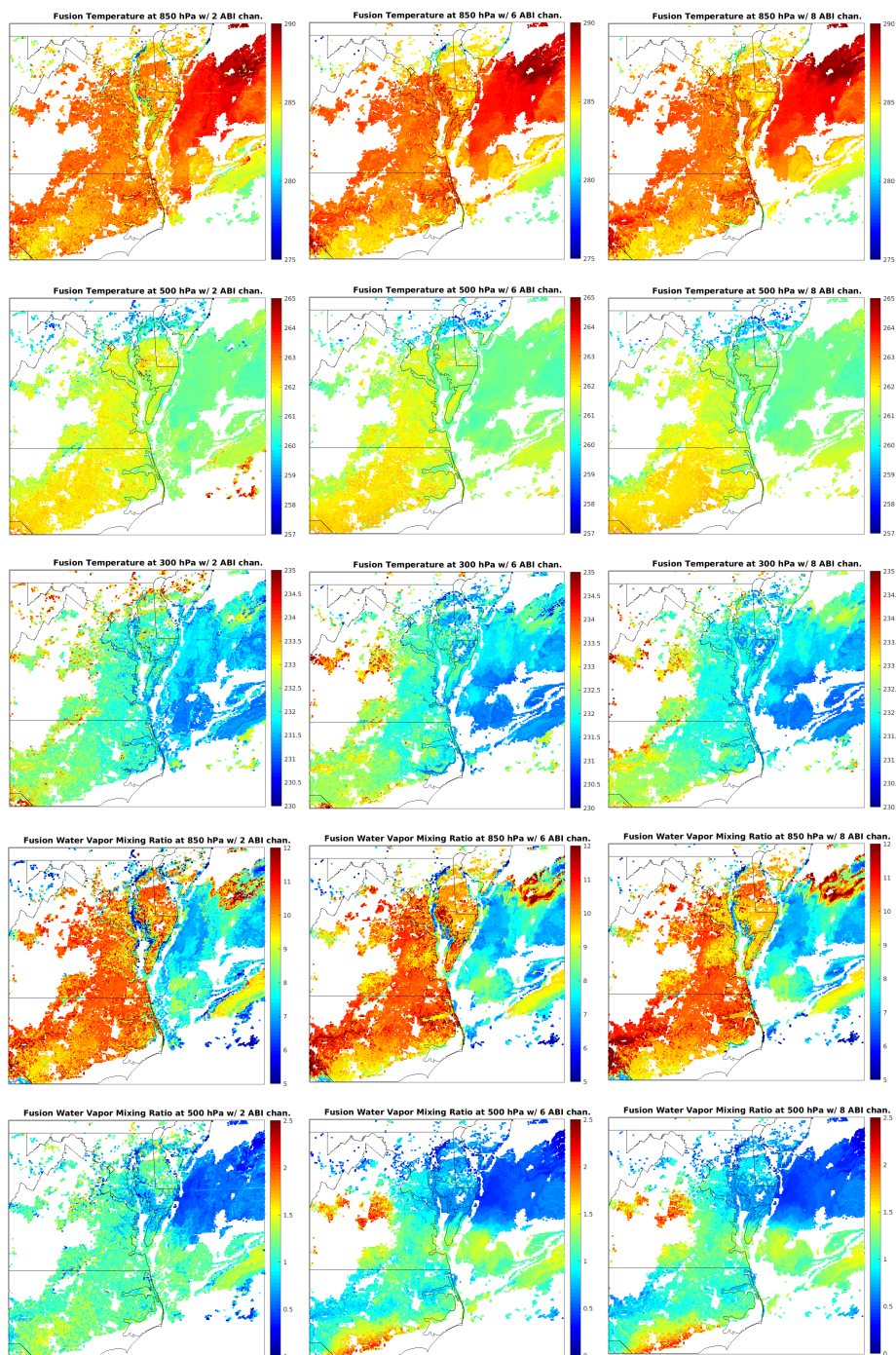


Figure 11: Fusion temperature at 850 hPa (top), 500 hPa (second from top) and 300 hPa (third from top) and fusion water vapor mixing ratio at 850 hPa (second from bottom) and 500 hPa (bottom) using two Advanced Baseline Imager (ABI) channels (14 and 15, left), six ABI channels (two channels plus 8, 9, 10 and 16, center) and eight ABI channels (six channels plus 11 and 12, right) over Chesapeake Bay using the Advanced Baseline Imager (ABI) image from 1800Z and the Cross-track Infrared Sounder (CrIS) data from the 1748Z and 1754Z granules. White signifies the presence of cloud at that pressure level. Additional channels in the fusion process improve the result.

Additionally, a land/sea separation was applied whereby an imager pixel is only allowed to match with sounder FOVs of the same land/sea status. This produced an unphysical land/sea discontinuity in the resulting retrievals and will not be applied in the rest of this work.

d. Product Fusion

The combination of parameters taken to be optimized for this application is a best match subset of $N=5$, a minimum clear best match requirement of minimum $N=2$ and the ABI input channel combination of 8, 9, 10, 11, 12, 14, 15 and 16 (Table 1). In this section, a summary of the resultant Chesapeake Bay, VA, May 19th, 2017 at 1800Z fusion retrieval dataset is presented in comparison with the original ABI and CrIS data from the same time. The data here illustrates the synergy of the high imager horizontal resolution and high sounder vertical resolution.

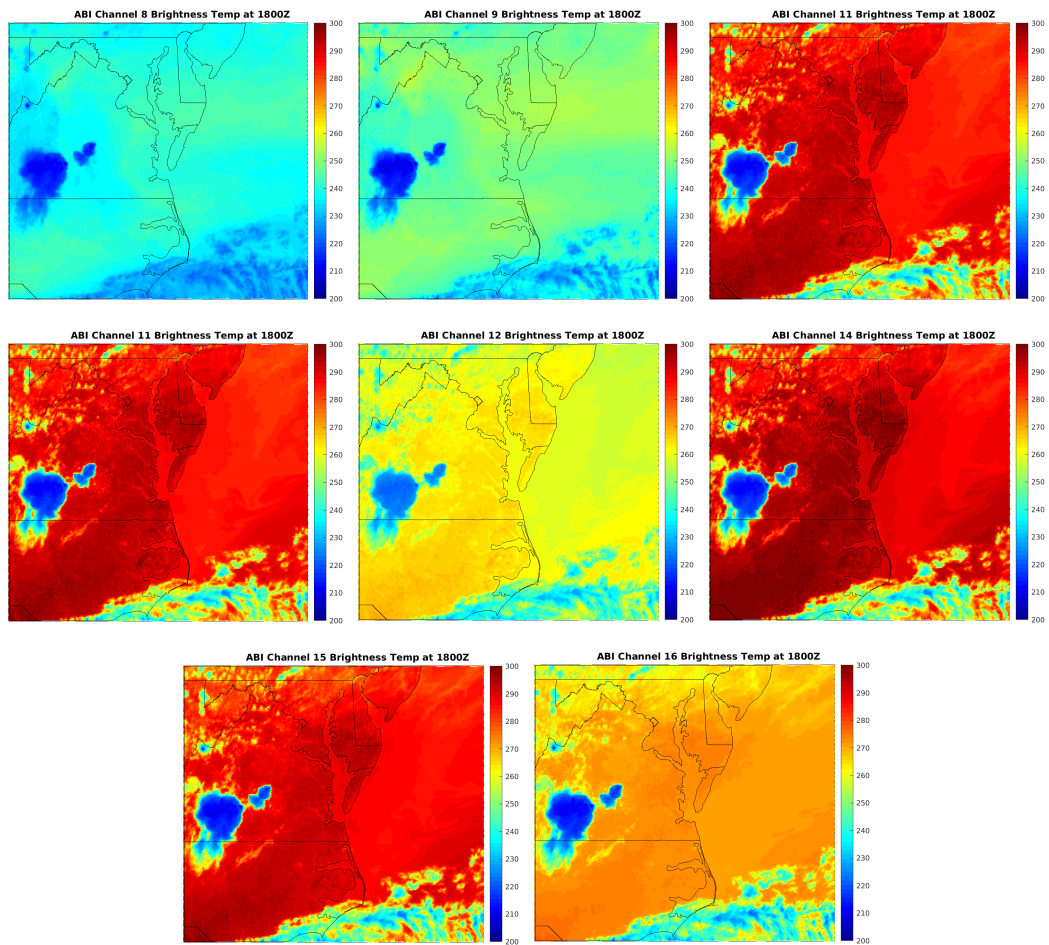


Figure 12: Advanced Baseline Imager (ABI) brightness temperatures from channels 8 (top left), 9 (top center), 10 (top right), 11 (middle left), 12 (middle center), 14 (middle right), 15 (bottom left) and 16 (bottom right) taken aboard Geostationary Operational Environmental Satellite (GOES)-16 over the Chesapeake Bay region at 1800Z on May 19th, 2017. These images serve as the imager input into the fusion process example shown here.

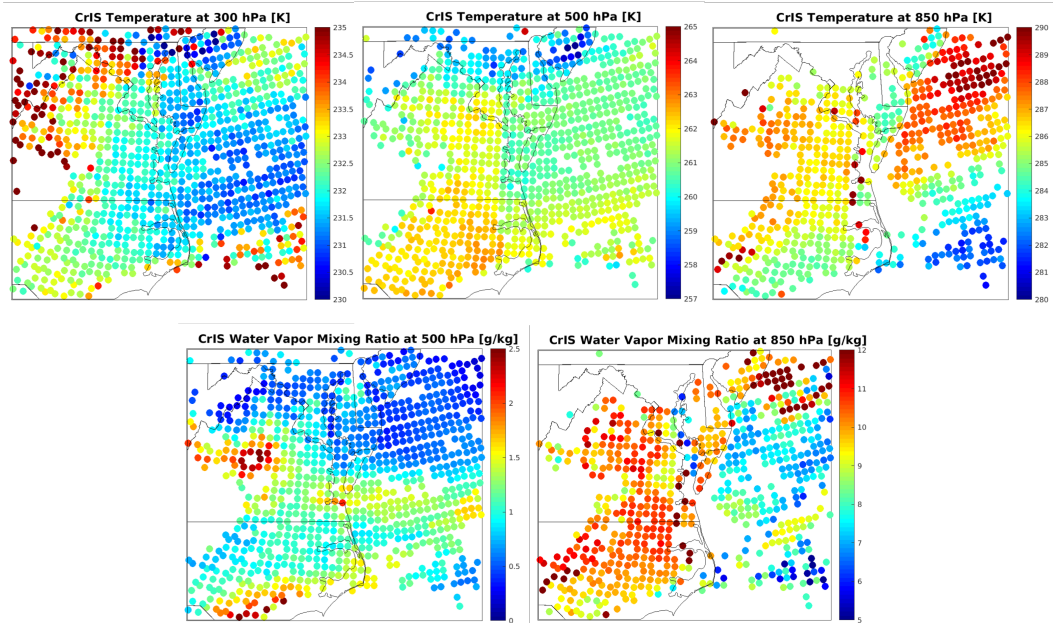


Figure 13: Cross Track Infrared Sounder (CrIS) derived temperature retrievals at 300 hPa (top, left), 500 hPa (top, center) and 850 hPa (top, right) and water vapor mixing ratio retrievals at 500 hPa (bottom, left) and 850 hPa (bottom, right) over the Chesapeake Bay region at 1754Z on May 19th, 2017 created using the University of Wisconsin Dual Regression (UW DR) retrieval algorithm [7]. These data serve as the sounder input into the fusion process example shown here.

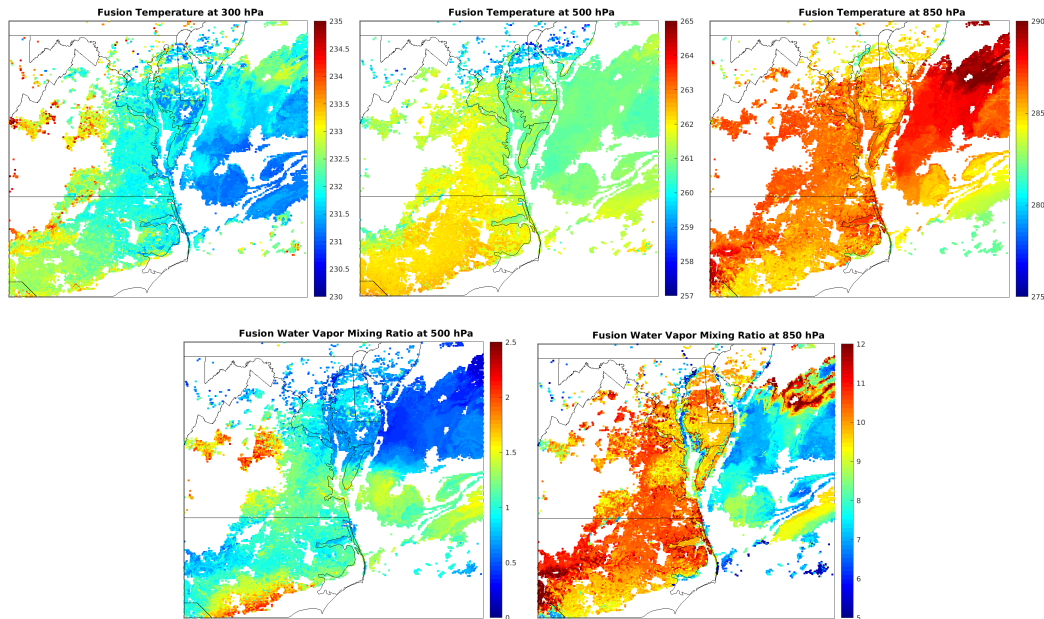


Figure 14: Fusion temperature retrievals at 300 hPa (top, left), 500 hPa (top, center) and 850 hPa (top, right) and water vapor mixing ratio retrievals at 500 hPa (bottom, left) and 850 hPa (bottom, right) over the Chesapeake Bay region at 1754Z on May 19th, 2017 created using the Advanced Baseline Imager (ABI) and University of Wisconsin Dual Regression (UW DR) retrieval algorithm [7] applied to Cross-track Infrared Sounder (CrIS) radiances.

The imager inputs into the fusion process are shown in Figure 12. The high spatial resolution of this information is immediately evident. As discussed, the spatial resolution is 2 km at nadir and 3–4 km over CONUS. We wish to retain this high spatial resolution in the final result. While these image inputs do not contain highly resolved vertical information, each channel does represent a particular atmospheric characteristic for the fusion process to train with. On the other hand, the sounder inputs (Figure 13) do contain highly resolved vertical information about the atmosphere but do not have nearly as high spatial resolution as the imager. The CrIS products used here were retrieved using the full spectral resolution data [9](2211 channels). Other combinations of imager/sounder instrument pairs and retrieval method capable of process hyperspectral sounder radiances may be used using the same fusion framework described here but are not presented herein. As discussed throughout this work, the

intent of this fusion process is to capture the high horizontal resolution of the imager and the high vertical resolution of the sounder.

Fusion retrievals using the $N=5$, minimum clear $N=2$ and eight channel search are shown in Figure 14. The fusion retrievals do indeed exhibit the high spatial resolution of the ABI imager as intended. Additionally, the products are “sounder-like” in that they do have vertical information and can yield profiles of temperature and water vapor.

Due to the somewhat interesting weather events occurring on May 19th 2017, a special radiosonde was launched at 1800Z from the National Weather Service Office in Wilmington, OH. This radiosonde data offers an opportunity to illustrate the vertical resolution of the fusion retrieval dataset and compare with the radiosonde and model data (Figure 15).

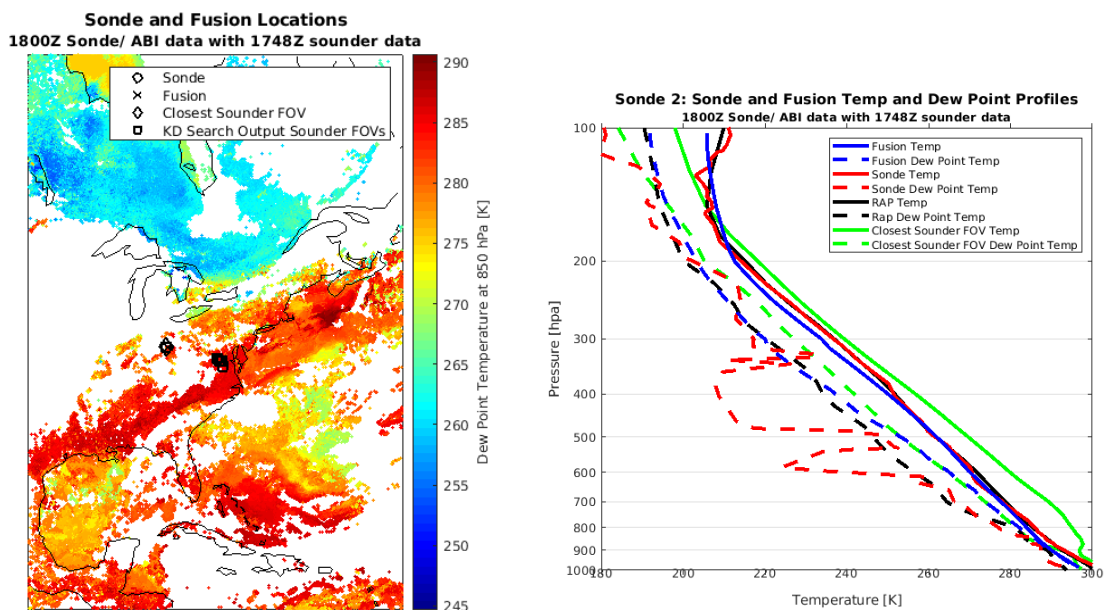


Figure 15: Locations of a special sonde launch, nearest fusion pixel, best match sounder fields of view (FOV)s and nearest CrIS FOV overlaid on 850 hPa dew point temperature at 1800Z on May 19th, 2017 over eastern North America (left). Vertical profiles of temperature and dew point temperatures of the special sonde, nearest fusion pixel, nearest CrIS FOV retrieval and National Centers for Environmental Prediction (NCEP) Rapid Refresh (RAP) model [22] nearest gridbox (right). The fusion profile matches the sonde more closely than the CrIS retrieval.

The plan view at left in Figure 15 shows the locations of the sonde launch site, nearest clear fusion (and ABI) pixel, nearest sonde FOV and best match sounder FOVs for the fusion pixel in question. The sonde, nearest fusion pixel and nearest FOV are all nearly collocated. The locations of the best match FOVs offer a glimpse into how the fusion process works. The best match FOVs are not necessarily located very near to the fusion pixel itself. The sounder FOVs in the vicinity of the fusion pixel are likely all cloudy. Additionally, the k-d tree search process searches for best matches in both radiance and geographic space. The best match FOVs that were selected may not be geographically close, but they must exhibit very similar radiance information to the fusion pixel in question.

The profile view at right in Figure 15 shows the first indications of the accuracy of the fusion process. The temperature and dew point temperature profiles are plotted for the fusion pixel, the radiosonde, the closest NCEP RAP model grid point and the nearest sonde FOV's retrieval. The temperature profiles for the fusion, sonde and model agree remarkably well. More interestingly, the nearest sounder FOV retrieval agrees much worse than the radiosonde. Fusion has very clearly done a much better job retrieving temperature at this point than the sounder retrieval. The model agrees best with the radiosonde when it comes to dew point temperature. In the lower troposphere, the sounder retrieval and fusion overestimate the dew point temperature. In the upper troposphere, the fusion dew point temperature agrees very well with the radiosonde while the sounder retrieval continues to overestimate.

e. Product Fusion Time Series

The high temporal resolution of the ABI imager allows for the creation of time series of retrieval fusion data. New GOES ABI images are available at a refresh rate of as high as one

minute inside one of two mesoscale regions over CONUS, 5 minutes over CONUS and 15 minutes over the entire disk [15]. In time series retrieval fusion creation, a fusion retrieval is created first using the same process as outlined above. The sounder data and imager data are taken to be very near concurrent in time and the resultant retrieval fusion data is considered to be “time step 0”. “Time step 1” occurs when the next ABI image is available for the region in question. At “time step 1”, a new retrieval fusion product is created using the same process as above and “time step 0” with one major modification. Rather than using the k-d tree to match each imager pixel with a subset of low resolution imager data created by geolocating with and averaging over a granule of sounder FOVs, the k-d tree is used to match each imager pixel with an imager pixel from the “time step 0”. This means every pixel in the new imager data from “time step 1” is matched with a subset of best match (in radiance and geolocation) imager pixels from “time step 0”. The corresponding fusion retrievals from the “time step 0” imager best match subset are then averaged together at every pressure level in order to form the new fusion retrieval data at “time step 1”. This process can be continued as new ABI data continuously becomes available at subsequent timesteps with each new imager pixel being matched with a subset of pixels from the previous image whose retrievals are then averaged to form the retrieval at the new time step. As before, the best match subset is taken to be of size $N=5$ and the minimum clear neighbors is taken to be minimum clear $N = 2$.

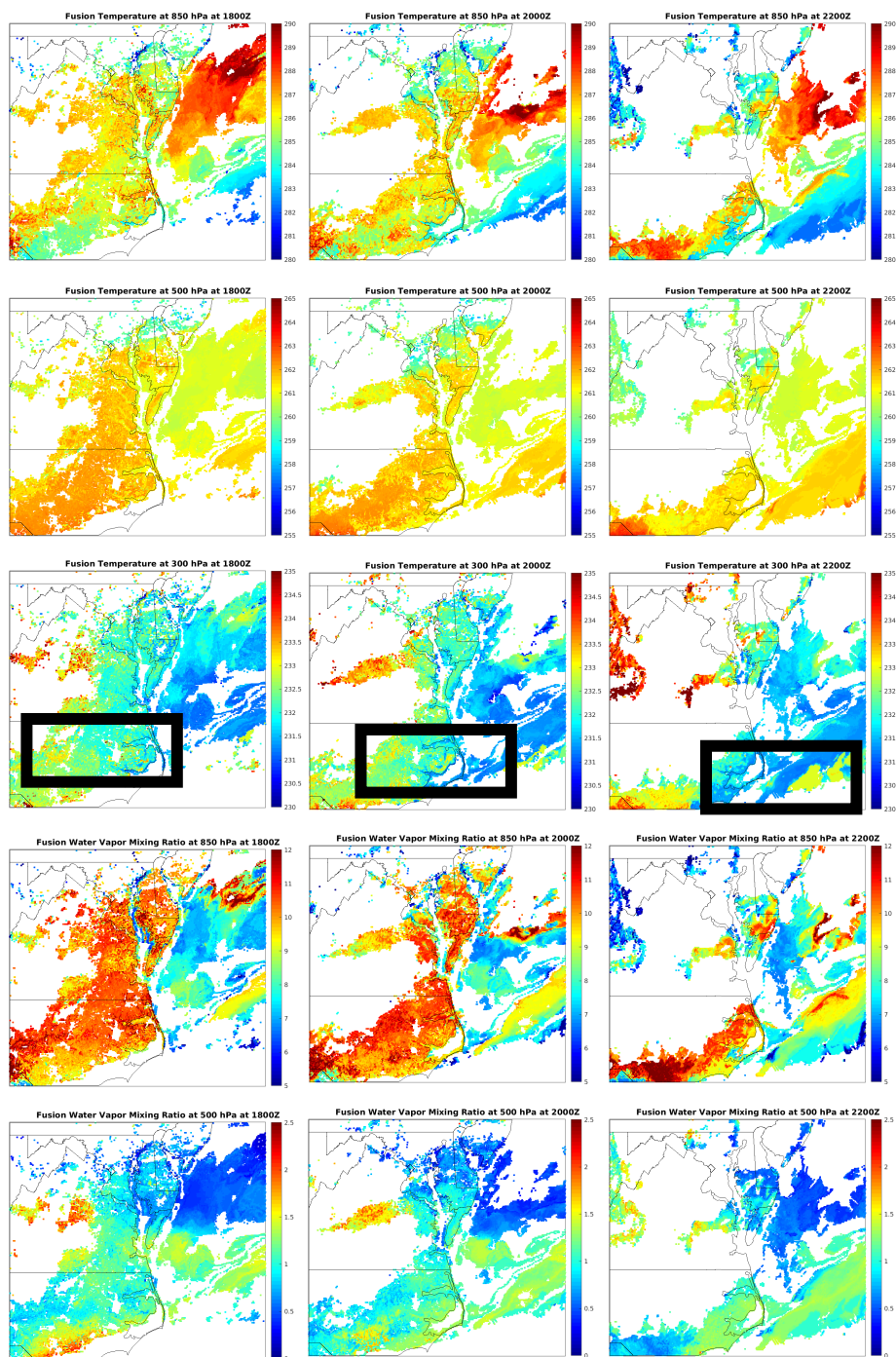


Figure 16: Fusion temperature at 850 hPa (top), 500 hPa (second from top) and 300 hPa (third from top) and fusion water vapor mixing ratio at 850 hPa (second from bottom) and 500 hPa (bottom) at 1800Z (left), at 2000Z (center) and at 2200Z (right) over Chesapeake Bay using the Advanced Baseline Imager (ABI) image from 1800Z and the Cross-track Infrared Sounder (CrIS) data from the 1748Z and 1754Z granules. White signifies the presence of cloud at that pressure level. Features in the atmosphere, especially convective lift shown by the 500 hPa temperature (bold box), can be followed over time.

Figure 16 shows an example time series created by completing the “time step 0” fusion at 1800Z and using the above procedure to create fusion retrievals at 2000Z and 2200Z. One can follow features in the atmosphere over these four hours by inspecting these retrievals. Of particular interest are the pockets of high temperature and water vapor exhibited in the upper levels in the pre-convective environments. In the 300 hPa fusion temperature retrieval, very high temperatures are retrieved in the regions ahead of the convection signifying uplift. This is a particularly interesting result and speaks to the potential for product fusion’s use in nowcasting settings. After this four hour period shown in Figure 16, the time series appears to break down. More work is necessary to determine for how long after the sounder overpass these time series retrievals can be trusted.

III. Validation

Radiosondes are commonly used as ground truth reference for validating satellite data products [25]. Here we used DOE ARM Southern Great Plains (SGP) site radiosonde launches that were collocated and concurrent with CrIS overpasses aboard Suomi NPP to develop mean and standard deviation error profiles for CrIS/ABI product fusion. The same statistics were calculated using RAP model data and CrIS UW DR to provide additional context. A very similar approach was used for validation of temperature and water vapor profile retrievals using the Atmospheric Infrared Sounder instrument in Tobin et. al, 2006. The radiosonde data used is from March 2017 to March 2018 with deployment coincident with Suomi NPP overpasses.

a. Radiosonde Dataset

Though radiosonde data has indeed been often used as validation for satellite derived profiles of the atmosphere, there are inherent limitations to doing so. There are many sources of error in radiosonde profile that must be considered when using them as ground truth.

First, the temporal limitations of a radiosonde must be considered. Whereas a satellite observation or fusion of satellite observations is taken to represent a singular moment in time, a radiosonde can take an hour or more to complete its observation through the desired depth of the atmosphere. During this time, the atmosphere very possibly may change significantly. This is especially true at the ARM SGP site from which the radiosondes used here were launched, owing to the dynamics of the mid-latitudes and this region specifically. During AIRS validation, two radiosondes were launched 60 minutes apart for each AIRS overpass in order to capture upper and lower atmosphere dynamics at the overpass time [26]. The differences between each pair of radiosonde launches was recorded in order to characterize the fluctuation in the atmosphere over 60 minute periods. The resultant differences are plotted in Figure 17 from Tobin, et al. 2006. The mean of the temperature and humidity differences is approximately 0 for the entire atmosphere for both daytime and nighttime cases. This is expected as the differences across 60 minutes should be random. The RMS of the temperature differences across 60 minutes was approximately .5 deg K for both daytime and nighttime cases. The humidity difference RMS is nearly 25% above 700 hPa for both daytime and nighttime cases and increases to over 35% in the upper atmosphere during day time cases. All of these values are significant compared to the stated AIRS accuracy goal of 1 deg K RMS within a 1km vertical layer below 100 mbar and 20% humidity RMS within a 2 km layer below 100 mbar [13] and also compared to the CrIS UW DR accuracy of 1 deg k and 20 % RH accuracy within a 1 km layer [20].

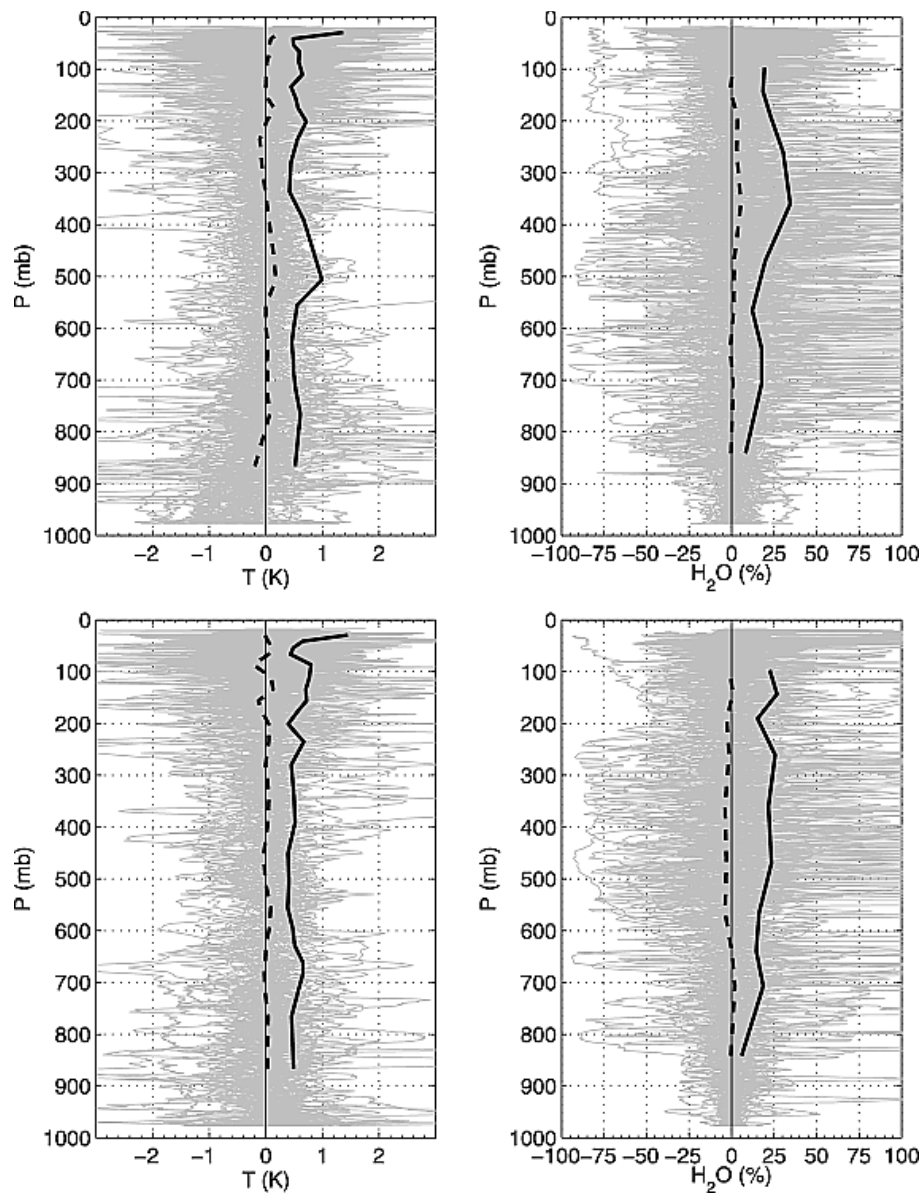


Figure 17: Temperature (left) and relative humidity (right) differences between sonde pairs launched ~60 minutes apart during day (top) and night (bottom) at the Department of Energy (DOE) Atmospheric Radiation Measurement (ARM) Southern Great Plains (SGP) site [21] during the validation campaign for the Atmospheric Infrared Sounder (AIRS). Adapted from Atmospheric Radiation Measurement site atmospheric state best estimates for Atmospheric Sounder temperature and water vapor retrieval validation by Tobin et al., 2006, Journal of Geophysical Research-Atmospheres, 111(D9), p. 18. These figures quantify the atmospheric variability a radiosonde can experience during the duration of its ascent through the atmosphere.

Owing to the extended amount of time a radiosonde needs to complete its observation along with the likelihood that winds will affect their vertical path, radiosondes are also limited in

their ability to provide a true vertical profile observation of the atmosphere. Throughout its trip through the depth of atmosphere, the horizontal location of a radiosonde is ever changing.

There are also well documented instrument errors associated with radiosondes. This error is typically well defined by the manufacturer and readily available. During the time period used for retrieval fusion validation, the Vaisala RS41 and Vaisala RS92 radiosonde models were used at the ARM SGP site. Their uncertainties are well defined by the manufacturer to be 0.4 deg K and 4% RH for the RS41 and 0.5 deg K and 5% RH for the RS92 [27].

To combat some of these potential error sources, best estimate profiles were created to compare the product fusion profiles to. Each best estimate profile is comprised of two radiosonde launches— one at roughly 45 min prior to satellite overpass and one at roughly 5 min prior to satellite overpass. The two radiosonde profiles are linearly interpolated to the overpass time at every pressure level in order to best represent the state of the atmosphere at the overpass time. The water vapor profile is scaled by a height independent factor such that the profile's total column precipitable water matches the total column precipitable water measured at the overpass time by a ground based, two channel microwave radiometer. Both of these strategies are similar to those described in [26].

b. Product Fusion Dataset

In order to create a statistical comparison between retrieval fusion and the radiosonde dataset, a retrieval fusion profile was created for every radiosonde. As such, there was a retrieval fusion dataset created for every CrIS overpass included in the radiosonde dataset.

For sounder/imager fusion validation, retrieval fusion was completed using the CrIS granule available with the start point nearest in time to the radiosonde launch and the GOES-16

ABI image from nearest in time to the radiosonde launch (either before or after radiosonde launch). The CrIS granule always includes the ARM SGP launch site. The fusion profile from the pixel nearest to the launch site was chosen for validation. This fusion profile is then compared with the radiosonde and RAP model at this location in order to arrive at the statistical comparisons shown in Figures 18 and 19.

c. Results

The fusion temperature profiles compare favorably with the sondes (Figure 18). In the lower and mid tropospheres, a bias of roughly -2 deg K is observed. The accompanying standard deviation in this layer is roughly 1 deg K. Both of these values are roughly twice the bias and standard deviation maximums found in a similar study using the UW DR algorithm applied to IASI radiances [7]. The mean difference and standard deviation between the nearest sounder FOV and the sonde profile are also plotted. The fusion statistics compare very well with this sounder/sonde profile.

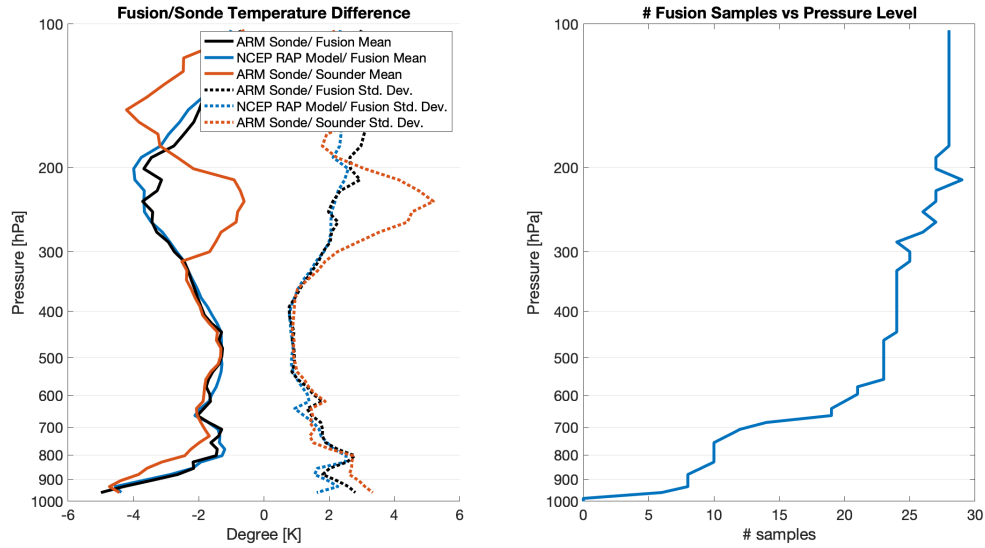


Figure 18: Left— Mean (solid) and standard deviation (dashed) of temperature differences versus pressure level for sonde and fusion (black), model and fusion (blue) and sounder and sonde (orange) from Feb. 2017- Feb. 2018 over DOE ARM SGP Site. Right— number of clear samples versus pressure level for the period in question. Temperature bias in the troposphere is $\sim -2\text{K}$ with a standard deviation of $\sim 2\text{K}$.

The fusion relative humidity retrievals also compare favorably with the sondes (Figure 19). In the lower troposphere, the bias appears to oscillate between 20% and 10% before setting around 0% in the upper troposphere with a standard deviation varying between about 25% and 10%. The bias results seem to perhaps be better than the values given in [7] for the UW DR algorithm while the standard deviation is very similar. Again, the sounder to sonde mean difference and standard deviation are plotted as well. The fusion statistics again compare well with these sounder/sonde values and may in fact be improved in the upper troposphere.

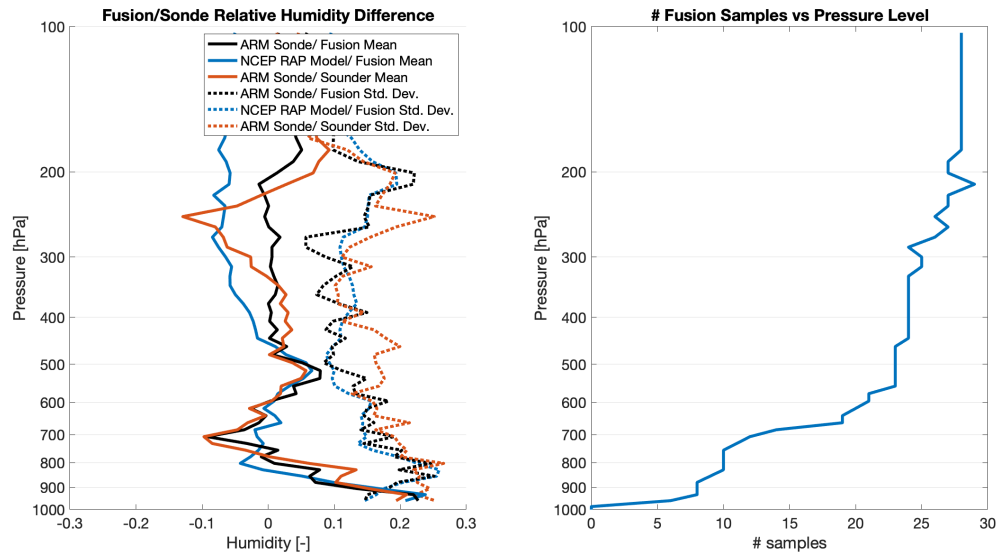


Figure 19: Left— Mean (solid) and standard deviation (dashed) of relative humidity differences versus pressure level for sonde and fusion (blue) and model and fusion (orange) from Feb. 2017- Feb. 2018 over DOE ARM SGP Site. Right— number of clear samples versus pressure level for the period in question. Relative humidity bias in the tropopause is ~ 0 with a standard deviation of $\sim 0.1\%$.

IV. Summary and Conclusion

Independently, modern infrared imagers and infrared sounders aboard Earth orbiting satellites exhibit unique advantages making them useful and important tools to today’s weather and climate monitoring industry. By identifying and utilizing an opportunity for synergy between the two types of instruments, the data fusion method demonstrated herein produces results exhibiting the unique advantages of both imagers and sounders while shedding their weaknesses. This fusion method has been previously proven to produce sounder like, narrow band radiances at imager like spatial resolution to supplement existing imager bands [19]. Here, we build upon a previous demonstration of product fusion [20] to further investigate how this method can best produce sounder-like, high vertical resolution retrieval products at imager horizontal and

temporal resolution. The combination of ABI aboard GOES-16 and CrIS aboard Suomi NPP is used to illustrate the process.

The method utilizes a k-d search tree method [23] to match each imager pixel over a given scene to a subset of best match sounder FOVs whose corresponding retrievals are averaged at every pressure level to construct the fusion retrieval. Increasing the size of that subset tends to smooth spatial variations in the result. A cloudmask can be applied to either the imager or sounder inputs or both, with the fusion process being applied only to the clear imager pixels. Varying the required number of clear subset sounder FOVs at a given pressure level from one to two for a fusion pixel to be deemed clear affects coverage area but also eliminates potentially erroneous results. Initially, the dirty window and window channels were used as inputs but adding the water vapor, cloud top phase, ozone and carbon dioxide channels [15] produced more structure in the results— particularly in water vapor.

By repeating the fusion process as new ABI images are available, product retrieval results can be available with high temporal resolution. By constructing a time series of hourly available fusion products, we can observe a storm system as it moves into pre-convective environments and watch as convection moves warmer air aloft. This data in particular provides a glimpse of the utility that a geostationary hyperspectral sounder would provide to the meteorology community.

We utilized the radiosonde launches associated with the CrIS validation campaign at the DOE ARM SGP site [21] to compare fusion results versus some form of ground truth. Best estimate profiles were constructed similar to [26] in order to produce the most accurate quantifications of temperature and water vapor profiles possible. When compared to these best estimate profiles, fusion performs well. Using 10 to 25 (varying with pressure level) clear sky

samples, the lower/mid troposphere fusion results show a temperature bias and standard deviation of roughly -2 K and 1 K respectively and a mid troposphere relative humidity bias of 0% with a standard deviation varying between 10% and 25% . The nearest CrIS FOV retrieval was also compared to each radiosonde best estimate profile— the fusion profiles were not any less accurate than these retrievals.

Data fusion between instrument pairs, like demonstrated here, is a useful tool when applied to instrument groups exhibiting synergy and could be used across remote sensing to provide observations with characteristics not possible with individual satellites. Particularly interesting is the opportunity for data fusion amongst smallsats and cubesats as they become more prevalent.

Bibliography

- [1] F. Castanedo, "A Review of Data Fusion Techniques," *Scientific World Journal*, p. 19, May 2013.
- [2] J. Cross, I. Gladkova, W. P. Menzel, A. Heidinger and M. Grossberg, "Statistical estimation of a 13.3 μm Visible Infrared Imaging Radiometer Suite channel using multisensor data fusion," *Journal of Applied Remote Sensing*, vol. 7, no. 11, 2013.
- [3] S. Miller, C. Schmidt, T. Schmit and D. Hillger, "A case for natural colour imagery from geostationary satellites, and an approximation for the GOES-R ABI," *International Journal of Remote Sensing*, vol. 33, no. 13, pp. 3999-4028, 2012.
- [4] F. Gao, J. Masek, M. Schwaller and F. Hall, "On the blending of the Landsat and MODIS surface reflectance: predicting daily Landsat surface reflectance," *Ieee Transactions on Geoscience and Remote Sensing*, vol. 44, no. 8, pp. 2207-2218, 2006.
- [5] C. S. Ruf, C. Chew, T. Lang, M. G. Morris, K. Nave, A. Ridley and R. Balasubramaniam, "A New Paradigm in Earth Environmental Monitoring with the CYGNSS Small Satellite Constellation," *Scientific Reports*, vol. 8, p. 13, 2018.
- [6] Y. Han and Y. Chen, "Calibration Algorithm for Cross-Track Infrared Sounder Full Spectral Resolution Measurements," *IEEE Transactions on Geoscience and Remote Sensing*, vol. 56, no. 2, pp. 1008-1016, 2018.
- [7] E. Weisz, W. Smith and N. Smith, "Advances in simultaneous atmospheric profile and cloud parameter regression based retrieval from high-spectral resolution radiance measurements," *Journal of Geophysical Research- Atmospheres*, vol. 118, no. 12, pp. 6433-6443, 2013.
- [8] W. L. Smith Sr., E. Weisz, S. V. Kireev, D. K. Zhou, Z. Li and E. E. Borbas, "Dual-Regression Retrieval Algorithm for Real-Time Processing of Satellite Ultraspectral Radiances," *Journal of Applied Meteorology and Climatology*, vol. 51, no. 8, pp. 1455-1476, 2012.
- [9] J. Le Marshall, J. Jung, J. Derber, M. Chahine, R. Treadon, S. Lord, M. Goldberg, W. Wolf, L. H. C., J. Joiner, J. Woollen, R. Todling, P. van Delst and Y. Tahara, "Improving Global Analysis and Forecasting with AIRS," *Bulletin of the American Meteorological Society*, vol. 87, no. 7, pp. 891-894, 2006.
- [10] M. G. Divakarla, C. D. Barnet, M. D. Goldberg, L. M. McMillin, E. Maddy, W. Wolf, L. Zhou and X. P. Liu, "Validation of Atmospheric Infrared Sounder Temperature and Water Vapor Retrievals with Matched Radionsonde Measurements and Forecasts," *Journal of Geophysical Research- Atmospheres*, vol. 111, no. D9, p. 20, 2006.
- [11] M. T. Chahine, T. S. Pagano, H. H. Aumann, R. Atlas, C. Barnet, J. Blaisdell, L. Chen, M. Divakarla, E. J. Fetzer, M. Goldbert, C. Gautier, S. Granger, S. Hannon and F. W. Irion, "Improving weather forecasting and providing new data on greenhouse gases," *Bulletin of the American Meteorological Society*, vol. 87, no. 7, p. 911, Jul 2006.
- [12] Y. Han, H. Revercomb, M. Crompton, D. Gu, D. Johnson, D. Mooney, D. Scott, L. Strow, G. Bingham, L. Borg, Y. Chen, D. DeSloover, M. Esplin, D. Hagan, X. Jin, R. Knuteson and H. Motteler, "Suomi NPP CrIS measurements, sensor data record algorithm, calibration

- and validation activities, and record data quality," *Journal of Geophysical Research- Atmospheres*, vol. 118, no. 22, pp. 12734-12748, 2013.
- [13] H. Aumann, M. Chahine, C. Gautier, M. Goldberg, E. Kalnay, L. McMillin, H. Revercomb, P. Rosenkranz, W. Smith, D. Staelin, L. L. Strow and J. Susskind, "AIRS/AMSU/HSB on the Aqua mission: design, science objectives, data products, and processing systems," *IEEE Transactions on Geoscience and Remote Sensing*, vol. 41, no. 2, pp. 253-264, 2003.
- [14] F. Hilton, R. Armante, T. August, C. Barnet, A. Bouchard, C. Camy-Peyret, V. Capelle, L. Clarisse, C. Clerbaux, P.-. F. Coheur, A. Collard, C. Crevoisier, G. Dufour and D. Edwards, "Hyperspectral Earth Observation from IASI: Five Years of Accomplishments," *Bulletin of the American Meteorological Society*, vol. 93, no. 3, pp. 347-370, 2012.
- [15] T. Schmit, M. Gunshor, W. P. Menzel, J. Gurka, J. Li and A. S. Bachmeier, "Introducing the next-generation Advanced Baseline Imager (ABI) on GOES-R,," *Bulletin of the American Meteorological Society*, vol. 86, no. 8, p. 1079, 2005.
- [16] D. Hillger, T. Kopp, T. Lee, D. Lindsey, C. Seaman, S. Miller, J. Solbrig, S. Kidder, S. Bachmeier, T. Jasmin and T. Rink, "First-Light Imagery from Suomi NPP VIIRS," *Bulletin of the American Meteorological Society*, vol. 94, no. 7, pp. 1019-1029, 2013.
- [17] M. D. King, W. P. Menzel, Y. J. Kaufman, D. Tanre, B.-C. Gao, S. Platnick, S. A. Ackerman, L. Remer, R. Pincus and P. A. Hubanks, "Cloud and aerosol properties, precipitable water, and profiles of temperature and water vapor from MODIS," *IEEE Transactions on Geoscience and Remote Sensing*, vol. 41, no. 2, pp. 442-458, 2003.
- [18] T. Schmit, R. Rabin, A. S. Bachmeier, J. Li, M. Gunshor, H. Steigerwaldt, A. Schreiner, R. Aune and G. Wade, "Many uses of the geostationary operational environmental satellite-10 sounder and imager during a high inclination state," *Journal of Applied Remote Sensing*, vol. 3, no. 22, 2009.
- [19] E. Weisz, B. A. Baum and W. P. Menzel, "Fusion of satellite-based imager and sounder data to construct supplementary high spatial resolution narrowband IR radiances," *Journal of Applied Remote Sensing*, vol. 11, p. 14, September 2017.
- [20] E. Weisz and W. P. Menzel, "Imager and sounder data fusion to generate sounder retrieval products at an improved spatial and temporal resolution," *Journal of Applied Remote Sensing*, vol. 13, no. 3, p. 12, July 2019.
- [21] G. M. Stokes and S. E. Schwartz, "The Atmospheric Radiation - Measurement (ARM) Program - Programmatic Background and Design of the Cloud and Radiation Tes-Bed," vol. 75, no. 7, pp. 1201-1221, 1994.
- [22] S. Benjamin, S. Weygandt, J. Brown, M. Hu, C. Alexander, T. Smirnova, J. Olson, E. James, D. Dowell, G. Grell, H. Lin, S. Peckham, T. L. Smith, W. Moninger and J. Kenyon, "A North American Hourly Assimilation and Model Forecast Cycle: The Rapid Refresh," *Monthly Weather Review*, vol. 144, no. 4, pp. 1669-1694, 2016.
- [23] J. L. Bentley, "Multidimensional binary search trees used for associative searching," *Communications of the ACM*, vol. 18, no. 9, pp. 509-517, 1975.
- [24] T. Schmit, J. Li, J. Gurka, M. Goldberg, K. Schrab, J. L. Li and W. Feltz, "The GOES-R Advanced Baseline Imager and the Continuation of Current Sounder Products," *Journal of Applied Meteorology and Climatology*, vol. 47, no. 10, pp. 2696-2711, 2008.

- [25] M. Feltz, L. Borg, B. Knuteson, D. Tobin, H. Revercomb and A. Gambacorta, "Assessment of NOAA NUCAPS upper air temperature profiles using COSMIC GPS radio occultation and ARM radiosondes," *Journal of Geophysical Research- Atmospheres*, vol. 122, no. 17, pp. 9130-9153, 2017.
- [26] D. Tobin, "Atmospheric Radiation Measurement site atmospheric state best estimates for Atmospheric Infrared Sounder temperature and water vapor retrieval validation," *Journal of Geophysical Research-Atmospheres*, vol. 111, no. D9, p. 18, 2006.
- [27] M. Jensen, D. Holdridge, P. Survo, R. Lehtinen, S. Baxter, T. Toto and K. Johnson, "Comparison of Vaisala radiosondes RS41 and RS92 at the ARM Southern Great Plains site," *Atmospheric Measurement Techniques*, vol. 9, no. 7, pp. 3115-3129, 2016.